Manipulation of magnetic anisotropy of Co ultrathin films by substrate engineering

Yuki Saisyu,[a] Toru Hirahara, Rei Hobara, and Shuji Hasegawa
Department of Physics, University of Tokyo, 7-3-1 Hongo, Bunkyo-ku, Tokyo 113-0033, Japan

(Received 8 March 2011; accepted 7 July 2011; published online 6 September 2011)

The magnetic and structural properties of Co films prepared on various substrates were investigated *in situ* based on the surface-magneto-optical Kerr effect (SMOKE) and using reflection high-energy electron diffraction (RHEED) and scanning tunneling microscopy (STM). The magnetic signals of the Co films were found to change significantly depending on the underlying substrates, the film thickness, and the temperature. Both STM and RHEED observations revealed that the shape and atomic structure of the Co islands were very different, which explains the observed magnetic anisotropy in SMOKE. We also observed a steep increase in coercivity for Co films thicker than 1.5 bi-layers grown on an Ag(111) film. This increase may be interpreted as a *fcc*-to-*hcp* structural transformation. © *2011 American Institute of Physics*. [doi:10.1063/1.3624662]

I. INTRODUCTION

Extensive studies have been conducted to examine the properties of nanometer-scale magnetic systems because of their importance in industrial fields of magnetism-based data storage media and possible applications to spintronics, such as spin valves.[1] In particular, the magnetic properties of thin magnetic films are an interesting area of research for future magneto-optic technology[2,3] and for the production of high-density hard disk drives.[4,5] The magnitude of magnetization, the coercivity needed in order for the field to reverse the magnetization, and the magnetic anisotropy, which determines the easy axis, are important parameters for practical applications. A number of systems of magnetic films have been fabricated by controlled epitaxial growth, and the magnetic properties of these films that are unique to low-dimensional systems have been investigated by various methods. The use of different substrates (on which the magnetic films grow) may be a relatively simple method by which to control/change these properties.

In the present study, we use three substrates, namely, a Si(111)- 7×7 clean surface, a Si(111)- $\sqrt{3} \times \sqrt{3}$ -Ag surface, and an Ag(111) surface, for the growth of magnetic materials (Co in the present study). The 7×7 surface is a complicated reconstruction having high-density dangling bonds on the topmost layer, which may be highly reactive with deposits, whereas the $\sqrt{3} \times \sqrt{3}$ -Ag surface has no dangling bonds and is likely to be inert.[6] The Ag(111) surface has no complicated reconstruction. Since these substrates give rise to different growth structures and have different wettability for magnetic materials, we expected that Co films grown on these substrates would exhibit different morphologies.

One of the most prototypical materials used in magnetic anisotropy study is Co, which has strong magnetic anisotropy because the Co bulk crystal forms a *hcp* uniaxial structure at room temperature (RT). A number of studies have been conducted using the surface-magneto-optical Kerr effect (SMOKE) method in order to evaluate the magnetic properties of thin Co films.[7–9] The morphology of the samples has also been investigated by scanning tunneling microscopy (STM).[10,11] However, few studies have systematically investigated the correlation between the magnetic properties and the structure/morphology of Co films.[12–14] Therefore, in the present study, we prepared ultrathin Co films on the three substrates, measured the magnetization curves *in situ* using SMOKE and observed their surface structures using STM and reflection-high energy electron diffraction (RHEED). We found a clear correlation between the Co film morphology/growth structures and magnetic properties.

II. EXPERIMENT

We used an *n*-type Si(111) wafer as a substrate and prepared three surfaces for the growth of Co films. The clean Si(111)- 7×7 surface was prepared by flashing the Si wafer by direct current at 1500 K in an ultrahigh vacuum (UHV). By the deposition of 1-ML Ag on the Si wafer at 650 K, a Si(111)- $\sqrt{3} \times \sqrt{3}$ -Ag surface can be formed.[6] A 12-atomic-layer-thick Ag(111) film was produced on the 7×7 surface by a typical method,[15,16] namely, Ag deposition at approximately 100 K with subsequent annealing up to RT. This process is known to be effective for producing an atomically flat and single-crystalline Ag(111) ultrathin film. The Ag coverage was determined by RHEED observation of the $\sqrt{3} \times \sqrt{3}$ -Ag pattern at 1 monolayer (ML).[6] After preparation of these surface super-structures or films, Co was deposited on the films at RT using an electron-beam evaporator. The Co coverage was monitored by the ion current measured in the evaporator, and the absolute value was determined by the formation of a Co/Si(111) super structure.[17] The basic unit of the Co *hcp* structure is one bi-layer (1 BL $= 3.66 \times 10^{15}$ cm^{-2}), which is equal to a Si atom density of 4.67 ML on a Si(111)- 1×1 truncated surface (1 ML $= 7.83 \times 10^{14}$ cm^{-2}).

These sample preparations, with the aid of RHEED, were performed on the upper level of the vacuum chamber of a recently developed UHV-SMOKE system.[18] The sample

[a]Electronic mail: yukisaisyu@surface.phys.s.u-tokyo.ac.jp.

was transferred to the lower level of the chamber in which the SMOKE measurements were performed *in situ* under a vacuum of 10^{-11} Torr. The sample can be cooled to as low as 15 K by flowing Liq-He into the sample holder. The magnetic field can be applied parallel to as well as perpendicular to the sample surface. These field alignments are referred to as the longitudinal (L-MOKE, //) and polar Kerr effect (P-MOKE, ⊥) measurements, respectively. The angle between the incident light and the sample is set to 45 degrees, so that the L-MOKE and P-MOKE have comparable sensitivity for the magnetization. They detect the sample magnetization parallel (perpendicular) to the sample surface. The field (up to ±0.23 T) was swept by symmetrically rotating a pair of SmCo permanent magnets placed on both sides of the sample, whereas the field direction with respect to the sample surface was changed by rotating the magnet pair around the sample.[18] The Kerr rotation angle was measured using the common Faraday-cell modulation technique along with a semiconductor laser beam (wavelength: $\lambda = 670$ nm). The angular resolution in the measurement was approximately 10^{-4} degrees.

When the film thickness d is much smaller than the laser wavelength λ, in the case of normal incidence, the complex Kerr rotation angle Φ_K is given by[19]

$$\Phi_K = \theta_K + i\eta_K = \frac{4\pi\varepsilon_{xy}d}{\lambda(n_s^2 - 1)\varepsilon_{xx}}, \quad (1)$$

where the real part θ_K is the Kerr rotation angle, the imaginary part η_K is the Kerr ellipticity, ε is the complex dielectric function of the magnetic film, and n_s is the refractive index. Since, in general, the off-diagonal element of the complex dielectric function ε_{xy} is proportional to the magnetization M, the Kerr rotation angle θ_K is also proportional to M. Consequently, we can obtain the magnetization curves of the magnetic film by monitoring θ_K when sweeping the external magnetic field.

The STM measurements were conducted in a separate UHV chamber (UNISOKU USM-501 type).[20] The samples were prepared *in situ* using RHEED in the same manner as in the SMOKE chamber. The base pressure was approximately 5×10^{-11} Torr. The STM measurements were performed at 65 K, although Co was deposited on the substrates at RT. All of the STM images shown here were captured in the constant current mode.

III. RESULTS AND DISCUSSION

A. Substrate dependence

Figure 1 shows the SMOKE measurement results for Co 1 BL films on the three substrates for (a) the longitudinal measurement (//) at RT, (b) the polar measurement (⊥) at RT, (c) (//) at 15 K, and (d) (⊥) at 15 K. The horizontal axis indicates the applied magnetic field, and the vertical axis indicates the measured Kerr rotation angle. In Fig. 1(a), a clear hysteresis loop appears only for the Ag(111) film, indicating that the sample is ferromagnetic. Thus, only Co on the Ag film is magnetized at RT, whereas the Co deposits on the other substrates are nonmagnetic. This result indicates that the magnetic properties of Co 1 BL films are significantly affected by the substrate. On the other hand, Fig. 1(b) indicates that there is only a marginal Kerr rotation in the perpendicular direction, even on the Ag film. This means that the easy axis is in-plane, i.e., the magnetization is parallel to the surface. Thus, the Co on the Ag film has prominent anisotropy, even at RT.

As shown in Fig. 1(c), when the sample is cooled to 15 K, the magnetization of Co on the Ag film is enhanced due

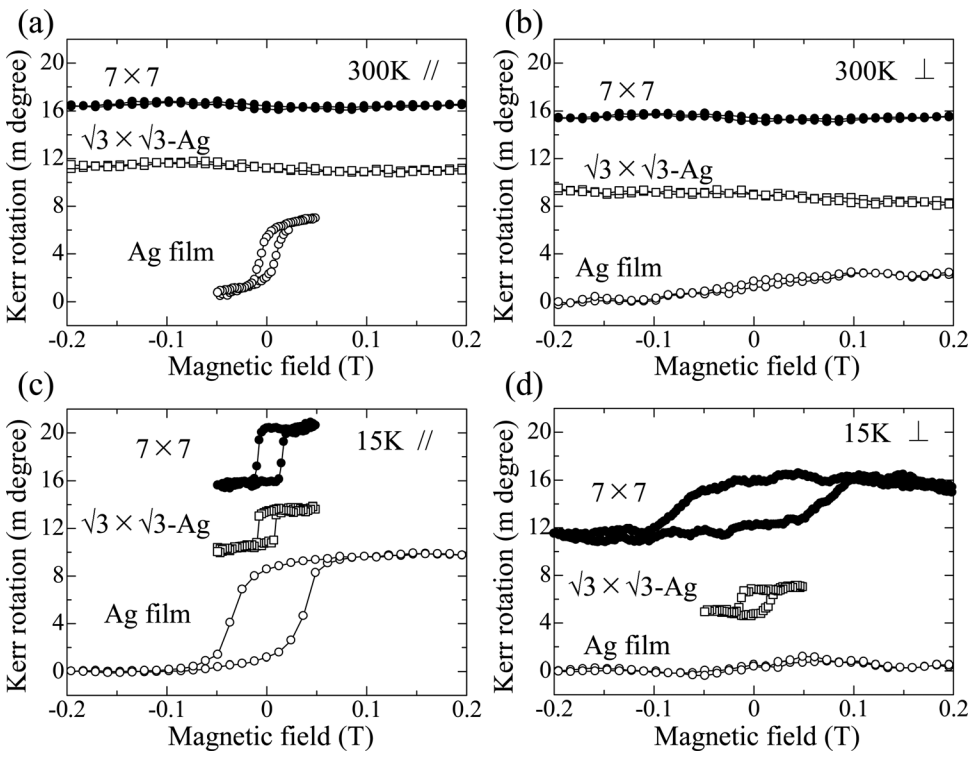

FIG. 1. SMOKE measurements of Co 1 BL films grown at RT on various substrates. (a) L-MOKE at 300 K, (b) P-MOKE at 300 K, (c) L-MOKE at 15 K, and (d) P-MOKE at 15 K. The closed circles indicate the data for the Co on the Si(111)- 7 × 7 surface. The quadrangles indicate the data for Co on the Si(111)- $\sqrt{3} \times \sqrt{3}$ -Ag surface, and the open circles indicate the data for Co on the Ag(111) film. The curves are vertically shifted for clarity.

to the suppressed thermal fluctuation, and the Co films on the other two substrates become ferromagnetic. This means that the Curie temperature of Co on these two substrates is below 300 K. We speculate that the formation of paramagnetic $CoSi_2$, which is known to grow at the initial adsorption of Co on the Si substrate, diminishes the magnetization[21,22] by forming a magnetic dead layer on the 7×7 and $\sqrt{3} \times \sqrt{3}$ -Ag surfaces, and ferromagnetic layers/islands are formed on top of the $CoSi_2$ layer. In fact, Co deposits on the two substrates have only half the Kerr rotation angles, as compared to the Co deposits on the Ag film. This is consistent with Eq. (1), which states that the Kerr rotation angle should be proportional to the magnetized thickness d in the film.

Moreover, cooling the sample enhanced the coercivity of Co on the Ag film. This is because more Zeeman energy is needed for magnetization reversal for moving the magnetic domain walls in the film since assistance by thermal energy for the domain wall movement is suppressed at low temperatures. Figure 1(d) also shows that Co on the Ag film does not exhibit any clear magnetization in the surface-normal direction, indicating clear in-plane magnetization. However, the Co on the 7×7 substrate exhibits a hysteresis loop and has a larger coercivity in the perpendicular direction than in the parallel direction shown in Fig. 1(c). In other words, it is easier to reverse the magnetization in the in-plane direction than in the perpendicular direction. On the other hand, Co on the $\sqrt{3} \times \sqrt{3}$ -Ag substrate does not exhibit any magnetic anisotropy, revealing similar coercivity fields and saturated magnetizations in both directions. Thus, the magnetic properties of 1 BL Co are very sensitive to the substrate for growth.

These results can be qualitatively understood based on the magnetic anisotropy energy (MAE) E_m, which is described by[23]

$$E_m = -\boldsymbol{B} \cdot \boldsymbol{M} + K_1 \sin^2 \theta + O(\sin^4 \theta) \tag{2}$$

where θ is the angle between the easy magnetization axis and the surface normal, B is the applied magnetic field, and M is the magnetization. In the case of a thin film,[24] the coefficient K_1 is given by

$$K_1 = -\frac{M^2}{2\mu_0}(N_z - N_x) + K_u + \frac{K_s}{d}, \tag{3}$$

where μ_0 is the permeability of the vacuum, N_z represents the perpendicular component of the demagnetizing coefficient, N_x is its in-plane component, and d is the film thickness. The first term is referred to as the shape anisotropy because the difference in demagnetizing coefficients between the x and z directions arises from the magnetic body shape. In addition, K_u represents the magnetic crystalline anisotropy energy, and K_s is the contribution from the surface (or interface).

The direction of the easy magnetization axis is determined in order to minimize the MAE. When K_1 is negative (positive), the easy axis would be parallel (perpendicular) to the surface. Since, based on the results in Fig. 1, the Co on the Ag film has $K_1 < 0$, K_1 should be dominated by the shape anisotropy term because, in the case of Co, K_u and $K_s \geq 0$.[25] On the other hand, Co on the $\sqrt{3} \times \sqrt{3}$ -Ag should not have any shape anisotropy, meaning that there is no preferential easy axis direction.

In order to confirm the above considerations concerning the shape anisotropy, we took STM images of the Co morphology on these substrates. As shown in Fig. 2, we found clear differences in the size and shape of the Co islands that grew on the three substrates. On the 7×7 surface (Fig. 2(a)), round islands of approximately 1 nm in size grew in an almost regular arrangement (Fig. 2(b)). Based on the line profile analysis, the width/height ratio of the Co islands is approximately 6 (Fig. 2(c)). Since Co is known to form a $CoSi_2$ paramagnetic layer at the initial stage of Co adsorption on the 7×7 surface at RT,[21] the islands in Fig. 2(b) are formed on the $CoSi_2$ wetting layer. This reduces the effective thickness of the magnetized Co layer.

Cobalt grows on the $\sqrt{3} \times \sqrt{3}$ -Ag surface (Fig. 2(c)) as smaller clusters (Fig. 2(e)). This is probably due to the dewetting tendency of the $\sqrt{3} \times \sqrt{3}$ -Ag surface. The width/height ratio of Co islands is approximately 3 (Fig. 2(f)).

In both cases of the 7×7 and $\sqrt{3} \times \sqrt{3}$ -Ag substrates, the RHEED pattern did not exhibit any diffraction spots/streaks/rings by Co adsorption. The 7×7 and $\sqrt{3} \times \sqrt{3}$ super-lattice spots just disappeared. This reveals the non-crystalline nature of the Co deposits.

In contrast, on the Ag(111) film (Fig. 2(g)), Co grows as distinctive patches as large as 10 nm in size (Fig. 2(h)), the width/height ratios of which are approximately 17 (Fig. 2(i)), which is much larger than in the other two cases. Thus, the Co islands on the Ag(111) film is the flattest, whereas the Co islands on the $\sqrt{3} \times \sqrt{3}$ -Ag surface are much more three-dimensional (3D). The Co islands on the 7×7 surface are intermediate between these two cases. As shown in the next subsection, the Co film on the Ag(111) film exhibited streaks in the RHEED pattern, indicating epitaxial growth of a single-crystalline Co film.

In summarizing this section, the magnetic moments at 15 K on the respective substrates are shown schematically in the insets of Figs. 2(c), 2(f), and 2(i). The observed magnetic anisotropy of Co films on the three types of substrates can be clearly explained by the STM results. Namely, the Co islands on the Ag(111) film are two dimensional, making the easy magnetization axis parallel to the surface due to the large positive value of $(N_z - N_x)$ in Eq. (3). On the other hand, the Co on the $\sqrt{3} \times \sqrt{3}$ -Ag surface has no obvious easy magnetization axis because the Co remains as small 3D particles with no shape anisotropy; $(N_z - N_x)$ is much smaller. Thus, the morphology (shape anisotropy) of the grown Co films governs the magnetic anisotropy.

B. Thickness dependence

We have demonstrated that 1 BL-thick Co on the Ag(111) film has prominent in-plane magnetic anisotropy. Next, we changed the Co thickness on this substrate and performed SMOKE measurements at RT. The hysteresis loops systematically changed with the Co thickness, as shown in Figs. 3(a) and 3(b). The longitudinal measurement (//) at RT (a) shows that the hysteresis loops become vertically

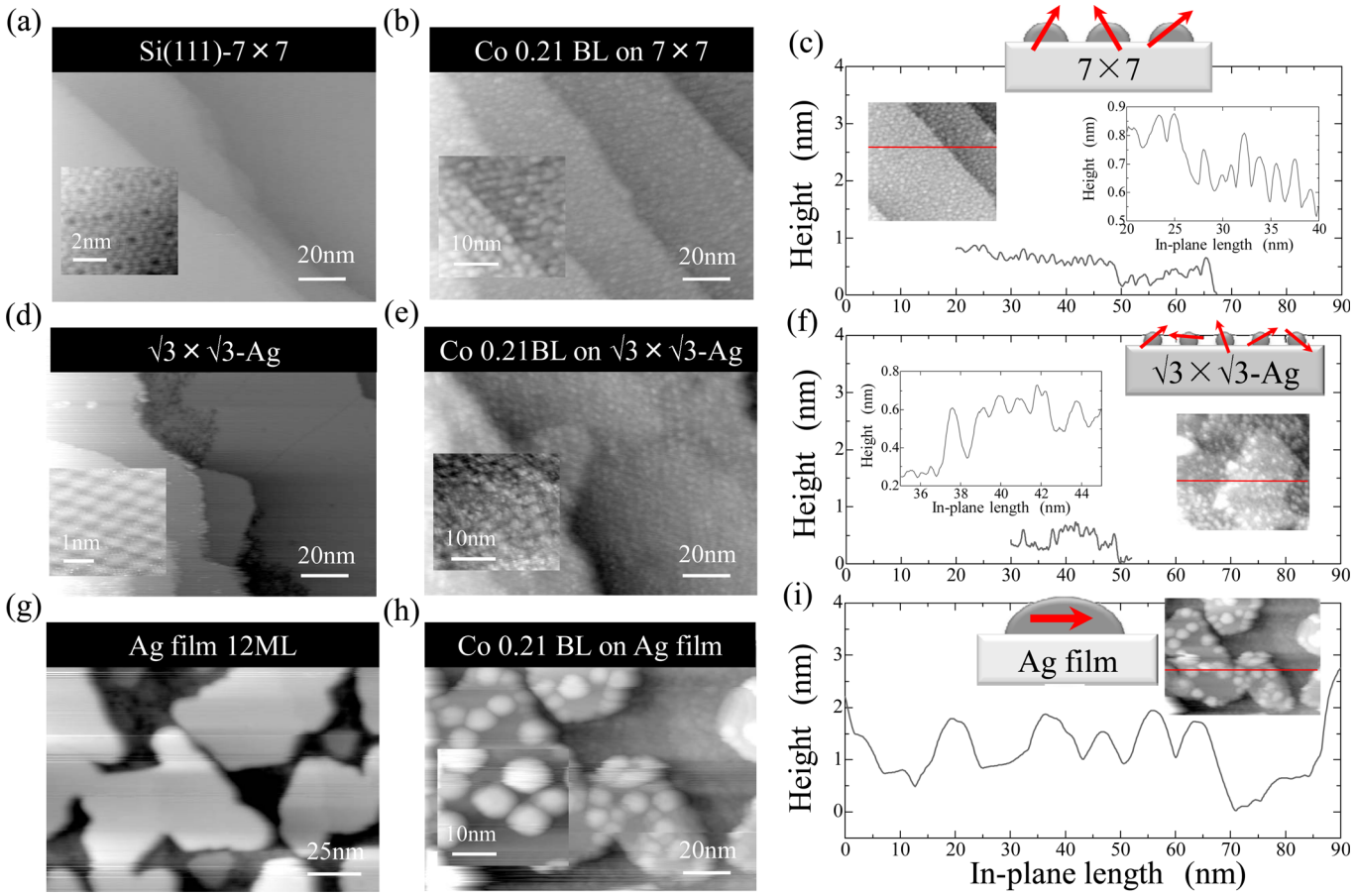

FIG. 2. (Color online) STM images of Co 0.21 BL on various substrates. (a) Si(111)- 7 × 7, (d) $\sqrt{3} \times \sqrt{3}$ -Ag surfaces, and (g) Ag(111) film before Co deposition. The images shown in (b), (e), and (h) are Co 0.21 BL deposited on the substrates shown in (a), (d), and (g), respectively. The graphs shown in (c), (f), and (i) present the line profiles for (a), (d), and (g), respectively. The magnified line profiles are also shown in (c) and (f). The inset schematics illustrate the structures and magnetization of the Co islands on the respective substrates.

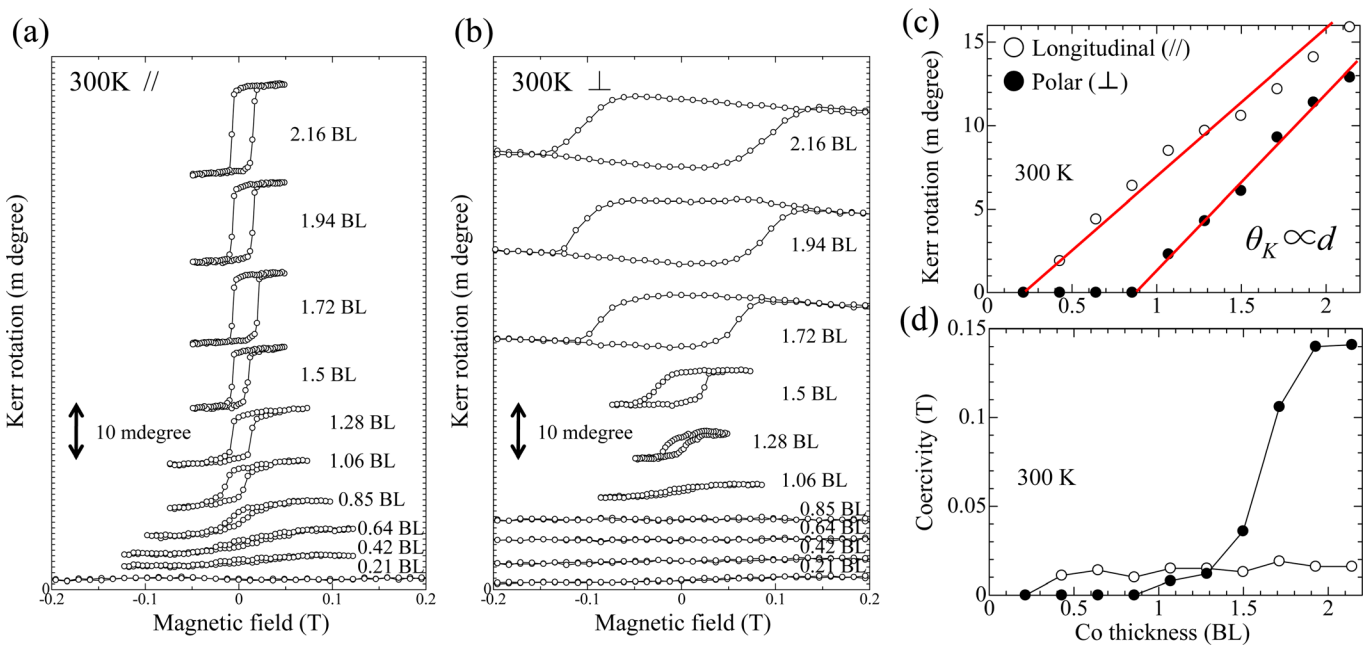

FIG. 3. (Color online) SMOKE measurements of different Co thicknesses on the Ag(111) film. (a) L-MOKE at 300 K, (b) P-MOKE at 300 K, (c) Kerr rotation angle, and (d) coercivity as a function of Co thickness. Open circles denote L-MOKE data, and closed circles denote P-MOKE data.

elongated as the thickness increases, whereas the horizontal width of the loop remains approximately constant. This means that only the Kerr rotation (θ_K) increases with thickness, whereas the coercivity B_c does not. In contrast, the polar measurements ($\perp$) at RT (b), show that the hysteresis loop expands horizontally as well as vertically with film thickness, which results in increases in the coercivity as well as Kerr rotation. Figure 3(b) shows that the Kerr rotation angle decreases with increasing magnetic field, but this does not mean that the polar magnetization decreases as well. This may possibly be due to the misalignment of the angle of incidence fixed to 45 degree that affects the mixing of the polar and longitudinal signal.[26]

Based on Figs. 3(a) and 3(b), θ_K and B_c are plotted as functions of Co thickness in Figs. 3(c) and 3(d), respectively. Figure 3(c) shows that perpendicular magnetization does not appear below 1 BL, whereas parallel magnetization is observable even at 0.42 BL. The increases in the Kerr rotation angle are linearly proportional to the film thickness d after the threshold thicknesses for both directions. A linear relationship with d is expected from Eq. (1). As shown in Fig. 3(d), the coercivity for the surface-parallel magnetization remains small and constant, irrespective of the Co thickness. However, that for the perpendicular magnetization begins to increase steeply for thicknesses over 1.5 BL. Thus, these results indicate that the magnetization is in-plane below thicknesses of approximately 1 BL, whereas it becomes out-of-plane above 1.5 BL. A magnetization reversal does not occur easily in the vertical direction, as compared with in the in-plane direction above 1.5 BL.

We also took STM images of some samples on the Ag film, as shown in Fig. 4. The insets show the RHEED patterns corresponding to the respective STM images. Figure 4(a) is an image of the Ag(111) film before Co deposition. Several flat terraces appear on the wetting layer (dark region). The RHEED pattern shows clear streaks (indicated by solid arrows) from the texture structure of the Ag(111)-1×1 face.[27,28] After 0.21 BL Co deposition, different streaks (indicated by dotted arrows in Fig. 4(b)) appear outside the Ag streaks. Since the ratio of streak spacing between the solid and dotted arrows is 1.15, which is approximately equal to the ratio between the Co(0001) lattice constant and that of Ag(111), we conclude that the outer streaks come from the Co. However, we cannot determine whether the structure is a *hcp* or a *fcc* structure because the *fcc* lattice constant is similar to the *hcp* lattice constant. Both the *fcc* and *hcp* structures of Co can be stable on noble metal (111) surfaces.[29–31]

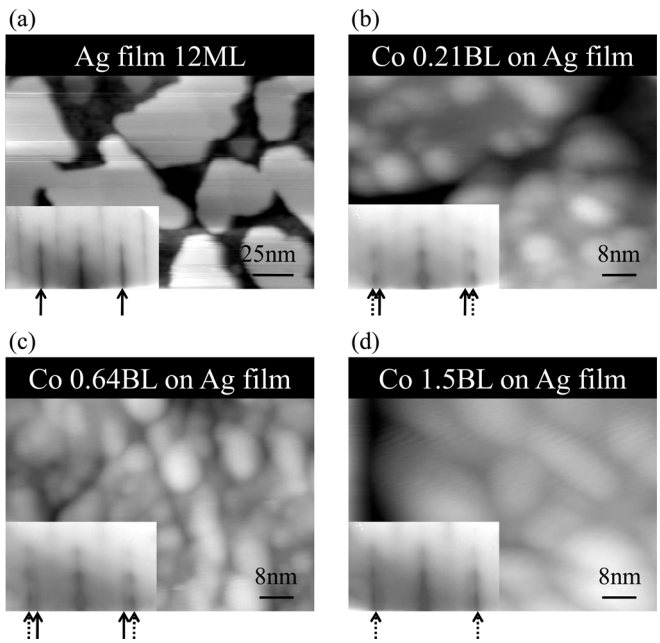

FIG. 4. STM images of different Co thicknesses on the Ag(111) film. (a) is a Ag(111) thick film before Co deposition, and (b), (c), and (d) are Co of 0.21, 0.64, and 1.5 BL, respectively, on the Ag(111) thick film. The insets show the RHEED patterns corresponding to the respective STM images. The dotted arrows indicate streaks coming from the Co, and the solid arrows indicate streaks coming from the Ag(111) substrate.

Figure 4(c) shows an image of 0.64 BL Co deposited on the Ag(111) film. Note that the Ag terraces are fully covered with Co islands. The island size does not change significantly, and the RHEED pattern shows similar streaks with some intensity modulation along the streaks, meaning a rough surface morphology.

The situation changes drastically above 1 BL. Perpendicular magnetization occurs at over 1 BL (Fig. 3(c)). We can infer this tendency from the fact that the easy axis of the bulk Co *hcp* structure is in [0001] direction, corresponding to the surface normal. This is reflected in the second term of Eq. (2). In fact, the easy axis of the thick Co film would ultimately be in the perpendicular direction because the shape and surface (interface) contributions (first and third terms in Eq. (3)) would diminish with the increase in thickness.

We interpret the changes in coercivity shown in Fig. 3(d) using a formula in which the coercivity B_c is described by the Stoner-Wohlfarth picture, namely, the *coherent rotation model*[32]

$$B_c = \frac{2K_u}{M_s} \tag{4}$$

or by the *global model*,[33,34]

$$B_c = \frac{\alpha\gamma}{M\nu^{1/3}} - \frac{N_{\mathrm{eff}}M}{\mu_0} - \frac{25k_BT}{M\nu},$$

where

$$\frac{\alpha\gamma}{M\nu^{1/3}} \approx \alpha\frac{K_u}{M_s}, \tag{5}$$

where M_s is the saturation magnetization, K_u is the magnetic crystalline anisotropy energy (as noted earlier), and the coefficients α and N_{eff} are experimental parameters. Both scenarios indicate that the coercivity is scaled by the ratio between K_u and M_s. Consequently, the drastic increase in coercivity in the perpendicular direction above 1.5 BL indicates a steep increase in K_u, because M_s remains approximately constant, as shown in Fig. 3(c) and Eq. (1). Why then does K_u begin to rise at a Co thickness of 1.5 BL?

This can be understood from the STM image and RHEED pattern in Fig. 4(d). At 1.5 BL, the Co streaks are dominant over the Ag streaks and no intensity modulation

occurs along the streaks, indicating a flatter Co surface. The STM image exhibits much larger islands than before. These results indicate that some structural transformation has occurred in the Co islands. If the transformation is a transition from a *fcc* structure to a *hcp* structure, exposing a (0001) surface on top, then the magnetic crystalline anisotropy energy K_u would abruptly increase due to the *hcp* uniaxial nature. This interpretation is consistent with the rapid increase in the perpendicular coercivity observed in Fig. 3(d). In fact, van Alphen *et al*. reported that a Co/Ag multilayer thin film is composed of *fcc-hcp* mixed crystals and transforms into the *hcp* structure at 5 ML in the *fcc* unit (which is equal to 2.4 BL in the *hcp* unit).[29] The result whereby the perpendicular coercivity saturates at approximately 2.1 BL agrees well quantitatively with the result reported by van Alphen *et al*. Thus, the structural transformation of Co films that occurred at around 1.5 BL affects the coercivity directly, producing the characteristic magnetic anisotropy.

IV. CONCLUSION

We have investigated the magnetic properties of Co films grown on various substrates using SMOKE. Co films on the Si(111)- 7×7 and - $\sqrt{3} \times \sqrt{3}$ -Ag surfaces had smaller Kerr rotation angles than the Ag(111) film due to the formation of $CoSi_2$ non-ferromagnetic layers during the initial stage of Co adsorption. On the Ag film alone, Co exhibited prominent in-plane magnetic anisotropy because of the relatively flat Co islands leading to the shape anisotropy, whereas Co on the $\sqrt{3} \times \sqrt{3}$ -Ag surface has no magnetic anisotropy because of the 3D shape of the Co clusters grown.

We varied the thickness of Co on the Ag(111) film. The magnetization was found to be in-plane for thicknesses of less than 1 BL, whereas it became out-of-plane for thicknesses greater than 1 BL. The coercivity parallel to the surface remained small, but the perpendicular coercivity increased sharply for thicknesses greater than 1.5 BL. These results are thought to be related to some sort of structural change, such as a *fcc*-to-*hcp* transformation, which induces strong crystalline magnetic anisotropy in order to cause the easy axis to be normal to the surface. The STM images and RHEED patterns also indicated such a change.

Through systematic investigations, we demonstrated that the magnetic anisotropy of ultrathin Co films is directly linked to the shape and atomic structure of the Co islands, which are influenced primarily by the substrate and the thickness of the grown film. The primary factor governing the magnetic anisotropy of the films changes from the shape anisotropy to the crystalline anisotropy as the Co film thickness increases.

ACKNOWLEDGMENTS

The present study was supported by a Grant-In-Aid (No. 19206006) from the Japan Society for the Promotion of Science. The SMOKE apparatus was developed in collaboration with UNISOKU Co., Ltd.

[1]S. A. Wolf, D. D. Awschalom, R. A. Buhrman, J. M. Daughton, S. von Molnár, M. L. Roukes, A. Y. Chtchelkanova, and D. M. Treger, Science **294**, 1488 (2001).
[2]W. B. Zeper, F. J. A. M. Greidanus, P. F. Garcia, and C. R. Fincher, J. Appl. Phys. **65**, 4971 (1989).
[3]J. Ferre, G. Penissard, C. Marliere, D. Renard, P. Beauvillin, and J. P. Renard, Appl. Phys. Lett. **56**, 1588 (1990).
[4]E. N. Abarra, B. R. Acharya, A. Inomata, and I. Okamoto, IEEE Trans. Magn. **37**, 1426 (2001).
[5]S. Iwasaki and K. Takemura, IEEE Trans. Magn. **11**, 1173 (1975).
[6]S. Hasegawa, X. Tong, S. Takeda, N. Sato, and T. Nagao, Prog. Surf. Sci. **60**, 89 (1999).
[7]Y. J. Wang, Z. H. Guo, D. K. Zhu, and C. H. Shang, J. Appl. Phys. **80**, 3957 (1996).
[8]P. Prod'homme, F. Maroun, R. Cortes, P. Allongue, J. Hamrle, J. Ferre, J. P. Jamet, and N. Vernier, J. Magn. Magn. Mater. **315**, 26 (2007).
[9]J. W. Lee, J. R. Jeong, and S. C. Shin, Phys. Rev. B **66**, 172409 (2002).
[10]K. Morgenstern, J. Kibsgaard, J. V. Lauritsen, E. Legsgaard, and F. Besenbacher, Surf. Sci. **601**, 1967 (2007).
[11]B. Voigtlander, G. Meyer, and N. M. Amer, Phys. Rev. B **44**, 10354 (1991).
[12]S. Rusponi, T. Cren, N. Weiss, M. Epple, P. Buluschek, L. Claude, and H. Brune, Nature Materials **2**, 546 (2003).
[13]W. Weber, C. H. Back, A. Bischof, C. Wursch, and R. Allenspach, Phys. Rev. Lett. **76**, 1940 (1996).
[14]H. Xu, C. H. Huan, T. S. Wee, and D. M. Tong, Solid State Commun. **126**, 659 (2003).
[15]L. Huang, S. J. Chey, and J. H. Weaver, Surf. Sci. **416**, L1101 (1998).
[16]I. Matsuda, T. Tanikawa, S. Hasegawa, H. W. Yeom, K. Tono, and T. Ohta, e-J. Surf. Sci. Nanotech. **2**, 169 (2004).
[17]A. E. Dolbak, B. Z. Olshanetsky, and S. A. Teys, Surf. Sci. **373**, 43–55 (1997).
[18]Y. Niinuma, Y. Saisyu, T. Hirahara, R. Hobara, and S. Hasegawa, e-J. Surf. Sci. Nanotech. **8**, 298 (2010).
[19]C. Y. You and S. C. Shin, J. Appl. Phys. **84**, 541 (1998).
[20]N. Sato, T. Nagao, and S. Hasegawa, Surf. Sci. **422**, 65 (1999).
[21]J. Derrien, M. De Crescenzi, E. Chainet, and C. d'Anterroches, C. Pirri, G. Gewinner, and J. C. Peruchetti, Phys. Rev. B **36**, 6681–6684 (1987).
[22]D. Shinoda and S. Asanabe, J. Phys. Soc. Japan **21**, 555 (1966).
[23]C. Zener, Phys. Rev. **96**, 5 (1954).
[24]M. T. Johnson, P. J. H. Bloemen, F. J. A de Broeder, and J. J. de Vries, Rep. Prog. Phys. **59**, 1409 (1996).
[25]F. J. A. den Broeder, W. Hoving, and P. J. H. Bloemen, J. Magn. Magn. Mater. **96**, 562 (1991).
[26]H. F. Ding, S. Putter, H. P. Oepen, J. Kirschner, J. Magn. Magn. Mater. **212**, 5 (2000).
[27]S. Hasegawa, H. Daimon, and S. Ino, Surf. Sci. **186**, 138 (1987).
[28]Y. Gotoh and S. Ino, Thin Sold Films **109**, 255 (1983).
[29]E. A. M. van Alphen and W. J. M. de Jonge, Phys. Rev. B **51**, 8182 (1995).
[30]M. T. Kief and W. F. Egelhoff, Phys. Rev. B **47**, 10785 (1993).
[31]F. J. A. den Broeder, D. Kuiper, A. P. van de Mosselaer, and W. Hoving, Phys. Rev. Lett. **60**, 2769 (1988).
[32]E. C. Stoner and E. P. Wohlfarth, Trans. Roy. Soc. (London) A **240**, 599 (1948).
[33]D. Givord, P. Tenaud, and T. Viadieu, IEEE Trans. Magn. **24**, 1921 (1988).
[34]D. Givord, Q. Lu, M. F. Rossignol, P. Tenaud, and T. Viadieu, J. Magn. Magn. Mater. **83**, 183 (1990).